PLD prepared bioactive $BaTiO_3$ films on TiNb implants

Miroslav Jelínek [a,b,*], Přemysl Vaněk [a], Zdeněk Tolde [c], Elena Buixaderas [a], Tomáš Kocourek[a,b], Václav Studnička [a], Jan Drahokoupil [a], Jan Petzelt [a], Jan Remsa [a,b], Marina Tyunina [d,a]

[a] Institute of Physics of the Czech Academy of Sciences, Na Slovance 2, 182 21 Prague 8, Czech Republic

[b] Czech Technical University in Prague, Faculty of Biomedical Engineering, nam. Sitna 3108, 212 01 Kladno, Czech Republic

[c] Department of Materials Engineering, Faculty of Mechanical Engineering, Czech Technical University in Prague, Karlovo náměstí 13, 121 35 Prague 2, Czech Republic

[d] Microelectronics Research Unit, Faculty of Information Technology and Electrical Engineering, University of Oulu, Finland

$BaTiO_3$ (BTO) layers were deposited by pulsed laser deposition (PLD) on TiNb, Pt/TiNb, Si (100), and fused silica substrates using various deposition conditions. Polycrystalline BTO with sizes of crystallites in the range from 90 nm to 160 nm was obtained at elevated substrate temperatures of (600 °C–700 °C). With increasing deposition temperature above 700 °C the formation of unwanted rutile phase prevented the growth of perovskite ferroelectric BTO. Concurrently, with decreasing substrate temperature below 500 °C, amorphous films were formed. Post-deposition annealing of the amorphous deposits allowed obtaining perovskite BTO. Using a very thin Pt interlayer between the BTO films and TiNb substrate enabled high-temperature growth of preferentially oriented BTO. Raman spectroscopy and electrical characterization indicated polar ferroelectric behaviour of the BTO films.

Introduction

Biomaterials are widely used for replacing irreversibly damaged tissues in the human body. They have to meet requirements for good functioning and long-term durability of the implants, namely biocompatibility, good corrosion and fatigue resistance, wear resistance and biomechanical compatibility [1]. An important requirement of implants designed to replace or interact with bone is a low elastic modulus matching as closely as possible to that of the

surrounding tissue [2]. Nowadays, Ti6Al4V alloy is frequently used for construction of implants because of low price and good mechanical properties [1].

Titanium and Ti6Al4V α-β alloys possess the lowest elastic modulus of the currently used surgical metals (~110 GPa); nevertheless, their stiffness is still high compared to that of human cortical bone (~20 GPa) [3]. The β-Ti alloys, and especially those based on Ti and Nb, have significantly lower elastic moduli and can become an attractive orthopaedic material [3].

Elastic modulus decreases to ~60 GPa at about 40 wt.% Nb for TiNb [4,5]. Titanium (Ti)-niobium (Nb) alloys have attracted much attention not only because of their non-toxicity, high corrosion resistance and beneficial mechanical properties [6–8], but also because of their high biocompatibility, i.e. improved cell adhesion and proliferation, particularly on their oxidized surfaces [9].

The electrical activity of biomaterials can improve their integration with the surrounding living tissue. It is well known that bone is electrically active under mechanical loading, due to the piezoelectricity of collagen [10,11] and the movement of ionic fluids within the bone structure (streaming potential) [12]. Electrical potentials in mechanically loaded bone have been linked to the mechanical adaptation of bone in response to loading [12–15], leading to the suggestion that the addition of an electrically active component to an implant material may improve healing and adaptation of the surrounding tissue. Recently, considerable interest has emerged to exploit this phenomenon to develop electrically active ceramics for implantation in hard tissue, which may induce improved biological responses [16,17].

In vivo studies of polarized hydroxyapatite ceramics have shown polarized samples to induce improvements in bone ingrowths [16,18]. Many piezoelectric ceramics proposed for implants are based on perovskite oxide ferroelectric barium titanate $BaTiO_3$ (BTO). In vivo and in vitro investigations have indicated that ceramics of this kind are biocompatible and, under appropriate mechanical load, induce improved bone formation around implants [16]. The mechanism by which electrical activity influences biological responses is not clearly understood, but it is likely to result from preferential adsorption of proteins and ions onto the polar surface.

Our work is aimed at coating TiNb implants (substrates) with ferroelectric $BaTiO_3$. It is known that the formation of the desired perovskite BTO phase requires high temperatures and oxygen-rich atmosphere, i.e., conditions under which intensive oxidation of the TiNb surface takes place. In order to avoid this unwanted oxidation, which prevents crystallization of chemically

and structurally pure BTO, an appropriate technology should be developed. Here the BTO films were prepared using PLD method. The deposition conditions, post-deposition processing, and multilayer design were varied and optimized with respect to phase composition, morphology, crystallinity, and polar properties of BTO.

Experimental

We have prepared BTO thin films using PLD. A high power KrF excimer laser (COMPexProTM 205 F, λ = 248 nm, τ = 20 ns) was used as an external source to vaporize the target material. The pressed BTO target pellet had 25 mm in diameter at a thickness of 5 mm. The films were prepared on one-side polished Ti-39 wt.% Nb, Pt/TiNb, Si (100) and fused silicasubstrates. β-Ti39Nb alloy samples were prepared by arc-melting 61 wt.% Ti (ingot, 99.55%, Frankstahl, Austria) with 39 wt.% Nb (ingot, 99.85%, TIC, Brussels, Belgium). The melting proceeded eight times at 800–1000 A/23 V with subsequent solution annealing at 850 °C for 30 min and water quenching to achieve the defined homogeneity.

The substrates for the TiNb layer were ground and polished. Using a SiC cutting wheel the as-prepared ingot was sliced into coupons (diameter of 10.5 mm and thickness of ~1 mm). The surfaces of the coupons were ground sequentially with abrasive papers (240, 600, 800, 1000 and 4000 grit) and then polished with a suspension of colloidal SiC (0.05 μm, Colloidal Sillicat, Leco, CR) into a mirror-like sheen, using a Leco machine.

Some films were subsequently post-annealed using rapid thermal annealing (RTA) method (Solaris 75, L&B Semiconductor) to recrystallize the layers after laser deposition.

Thickness and roughness of layers were measured by an Alpha-step IQ mechanical profilometer (KLA TENCOR Co.). The uncertainty in the thickness estimation is about 10% in the examined range of thicknesses, partly due to the fact that the layer thickness in the centre of the sample is higher than at its edges.

Film morphology was checked by scanning electron microscope Jeol JXA-733.

We used XRD in two different arrangements and sources: with divergent beam (Bragg Brentano) and with parallel beam. The reason was to find wider scale of conditions to determine preferred orientations. The first one uses a parallel beam geometry, Cu radiation (0.154056 nm), a detector scan with the stationary sample (rotating around the normal to the surface), and the glazing angle of incidence (GAOI). The second one uses a Bragg-Brentano geometry with a linear X'Celerator detector, the Co radiation (λ = 0.178901 nm). The samples were inclined by 5° from ideal position to avoid diffraction from single crystal substrate. The diffraction patterns

were evaluated by Rietveldlike program TOPAS 3 [19]. In this method the measured diffraction pattern is compared with the calculated one and the input parameters are varied on the basis of differences between the measured and calculated diffraction pattern. For the calculation of diffraction pattern, the program is using the so-called "fundamental parameter approach" [20], i.e. the calculated diffraction profile is based on convolution of particular contribution to diffraction profile. Three components of diffraction peak broadening are taken into account: the instrumental broadening, average crystallite size and microstrains. In this way, precise determination of the average crystallite sizes and microstrains is possible. Microstrains e describe the fluctuation of inter-planar distance d and are defined as Δd/d [21]. Moreover, the Rietveld base procedure gives also the lattice parameters and eventually phase composition.

The Raman spectra were excited on the optically polished samples with the 514.5 nm line of an Ar-laser at a power of 20 mW and recorded in back-scattering geometry using an RM-1000 RENISHAW Raman Microscope equipped with a Bragg filter. The diameter of the laser spot on the sample surface amounted to 2–3 μm, and the power on the samples was about 4 mW.

For electrical characterization of the BTO films, thin-film capacitors were formed by pulsed laser deposition of the Pt top circular electrode pads using shadow masks. As a bottom electrode, either the TiNb substrate itself or additional Pt layer was employed. The area of capacitors was 0.2–12 mm^2. The polarization, leakage current, capacitance, and loss factor were measured by a TF2000 Analyzer (aixACCT Systems GmbH). The capacitance-voltage characteristics were acquired using superposition of dc biasing voltage and small ac probing signal.

Results and discussion

The goal was to prepare ferroelectric thin films on TiNb substrates. At first we have tried to fabricate crystalline BTO films on TiNb, for target-substrate distance d_{T-S} = 35 mm and two values of the oxygen pressure (1 Pa and 20 Pa). We varied substrate temperature (T_S) from 200 °C to 900 °C

Layers were amorphous for deposition temperatures T_S up to ~500 °C. With increasing temperature T_S, the formation of perovskite BTO was achieved, which, however, was accompanied by profound growth of rutile. The X-ray diffraction (XRD) revealed the presence of (001), (101), (111), and (002) BTO diffractions, (110) and (211) rutile (TiO_2) diffractions and also some unidentified diffractions. The intensity of the BTO diffractions was the highest

at 700 °C and decreased with increasing T_S, whilst the inverse trend was observed for the rutile. With increasing T_S to 900 °C, also oxygen deficient titania phases were detected.

For the best crystallized BTO (T_S = 700 °C, oxygen pressure of 1 Pa), the ratio of intensity of diffractions (100)/(111) was approximately 0.17, compared with that of 0.625 in the bulk (ICDD Card No. 5-626, 211276, 23-1078). This observation suggests tendency to preferential (111) oriented growth of the BTO films (Fig. 1). Raman spectroscopy has not revealed any features typical for bulk BTO in these films (Fig. 2).

The formation of rutile is most probably related to oxidation of the TiNb substrate during the high-temperature deposition using oxygen atmosphere. In order to cut uncertainty related to technological process as a possible reason for rutile formation, BTO films were prepared using Si (100) and on amorphous fused silica as substrates. Phase-pure well crystallized BTO films were obtained on these substrates (Figs. 3 and 4).

The BTO films were deposited on Si (100) substrates using T_S of 700 °C, $d_{T\text{-}S}$ of 6 cm, and two different energy densities: 2 J cm^{-2} and 4 J cm^{-2}. The crystal structure of the BTO films was very similar. The intensity ratio (100)/(111) was 3.58 (for 2 J cm^{-2}) and 3.42 (for 4 J cm^{-2}), suggesting tendency to preferential (001) orientation. The average crystallite size and microstrain are 89 nm vs 160 nm, and 0.20% vs 0.15% in the sample prepared at 4 J cm^{-2} vs sample prepared at 2 J cm^{-2}, correspondingly. This observation shows better crystallinity of the prepared at 2 J cm^{-2}.

These films exhibited typical BTO modes in their Raman spectra, too (Fig. 5). A slight shift of the mode frequencies compared with those in ceramic BTO can be related to mechanical stress in the films on Si (100) (see cracks in the photograph, inset Fig. 5). Somewhat better crystallization is found in the films obtained at energy density of 2 J cm^{-2}.

Using amorphous fused silica substrates allowed us to get rid of cracking (Fig. 6). BTO polycrystalline films were formed at 700 °C only, whilst lower deposition temperatures were insufficient for crystallization – see Fig. 4. Interestingly, the films deposited at lower oxygen pressure of 0.1 Pa compared with 10 Pa were better texturized with preferred (100) orientation and with larger lattice parameters. However, such films did not exhibit typical BTO features in the Raman spectra, indicating possible off-stoichiometry (oxygen deficiency) therein, Fig. 7.

Our experiments demonstrated that oxidation of the TiNb substrate during high-temperature BTO deposition is the most likely reason for the formation of unwanted titania phases, preventing perovskite BTO crystallization. In order to avoid or reduce titania formation,

amorphous BTO was first deposited on TiNb at low T_S. The BTO crystallization was achieved using the rapid post-deposition annealing. The 10 samples of 200 nm thick amorphous BTO films were prepared at T_S = 160 °C, in 1 Pa of oxygen and fluence of 2 J cm^{-2}. The BTO films were annealed under various conditions (set of very short pulses to a single pulse of 5 min for T_S of 500 °C to 900 °C). The Raman FE BTO peak was found on only one post-annealed BTO film (annealing at 700 °C for 4 min). The corresponding XRD structure exhibited (100)/(111) ratio of 0.32 – see Fig. 8. The Raman FE peak is shown in Fig. 9.

The electrical characterization of this film (capacitor area 0.2 mm^2) revealed a bell-shaped capacitance-voltage curve, which is generally typical for the paraelectric state or non-linear dielectric (Fig. 10a). However, the presence of minor hysteresis is also observed, suggesting that the film can contain ferroelectric fraction. The relatively large leakage current and loss factor tan D point to substantial conductivity of the film (Figs. 10b, c). Interestingly, the current vs voltage curve exhibits hysteresis, also indicating the presence of ferroelectric fraction. Because of possible coexistence of ferroelectric BTO and other phases, small sizes of grains, and random orientation of BTO crystallites, the polarization and dielectric response of the BTO film are not of pure ferroelectric character.

Importantly, significant further improvements in crystallinity and properties of the BTO films are obtained by using a thin Pt interlayer between the TiNb substrate and the BTO film. The two Pt layers – bottom and top – were deposited by PLD (see scheme in Fig. 11).

BTO layers were prepared at T_S of 700 °C, at two oxygen pressures: 10 Pa and 0.1 Pa. Films were very smooth – see Fig. 12. The XRD revealed only crystalline BTO phases - see Fig. 13. The (100)/(111) ratio was 0.16 (for 10 Pa of oxygen) or 0.75 (for 0.1 Pa of oxygen). Raman spectroscopy revealed FE BTO mode in the film deposited at high oxygen pressure (10 Pa), but not in the film deposited at lower oxygen pressure (0.1 Pa), Fig. 14.

Interestingly, the BTO film deposited at low oxygen pressure and lacking clear ferroelectric features in the Raman spectrum, exhibits, nevertheless, very large and strongly tunable capacitance (Fig. 15a). Also the observed capacitance-bias hysteresis indicates a ferroelectric-like response of this film. The achieved capacitance density is approximately 15 nF/mm^2 at zero bias, which is very large. It can be tuned by dc voltage: the capacitance decreases by a factor of 2 with increasing bias to 6 V only. These interesting dielectric properties are combined with satisfactory leakage and loss characteristics.

The FE BTO mode in the Raman spectrum of the film deposited at high oxygen pressure (10 Pa) suggests that this film should exhibit ferroelectric behavior. Indeed, compared with the film prepared at 0.1 Pa, the film demonstrates smaller capacitance and better expressed hysteresis in capacitance and current: the features pointing to more ferroelectric-like response. It is, however, impossible to claim that the film is pure ferroelectric based on these observations. We note that measurements of polarization in all of the samples were restricted by large conduction currents in the capacitors. Although there is no clear evidence of macroscopic ferroelectric response, the results in Fig. 15 imply that the films contain ferroelectric fraction.

Conclusions

Thin BTO films were deposited by PLD method on TiNb, Pt/TiNb, Si (100) and fused silica substrates using various deposition conditions. Polycrystalline perovskite BTO was obtained on TiNb at high deposition temperatures (T_S ~ 700 °C and higher), which led to concurrent formation of unwanted rutile. In order to avoid rutile formation and to enhance perovskite BTO crystallization, two strategies were implemented. In the first approach, amorphous layers were deposited on TiNb at temperatures lower than 500 °C and they were subjected to post-deposition rapid thermal annealing. In the second approach, thin Pt interlayer was deposited on TiNb implant, and the BTO film was then grown at high temperature and oxygen pressure, in order to obtain perovskite BTO crystallization. The formation of perovskite phase and presence of ferroelectricity are evidenced by XRD analysis, Raman spectroscopy, and electrical characterization. Further optimisation of deposition process and multilayer design is still desirable.

Acknowledgements

The work was supported by the Grant Agency of the Czech Technical University in Prague, grant No. SGS14/168/OHK4/2T/17 and by Grant Agency of the Czech Republic (grant GA-15-01558S and GA-15-05864S).

References

[1] M. Geethaa, A.K. Singhb, R. Asokamania, A.K. Gogia, Ti based biomaterials, the ultimate choice for orthopaedic implants – a review, Prog. Mater. Sci. 54 (3) (2009) 397–425.

[2] D.A. Pueblo, A. Nancy, Understanding and controlling the bone-implant interface, Biomaterials 20 (1999) 2311–2321.

[3] R. Godley, D. Starosvetsky, I. Gotman, Corrosion behavior of a low modulus beta-Ti45%Nb alloy for use in medical implants, J. Mater. Sci. Mater. Med. 17 (2006) 63–67.

[4] S. Hanada, H. Matsumoto, S. Watanabe, Mechanical compatibility of titanium implants in hard tissues, Int. Congr. Ser. 1284 (2005) 239–247.

[5] Y.B. Wang, Y.F. Zheng, The microstructure and shape memory effect of Ti-16 at.%Nb alloy, Mater. Lett. 62 (2) (2008) 269–272.

[6] R. Olivares-Navarrete, J.J. Olaya, C. Ramírez, S.E. Rodil, Biocompatibility of niobium coatings, CoatingsTech 1 (2011) 72–87.

[7] D. Velten, E. Eisenbart, N. Schanne, Biocompatible Nb_2O_5 thin films prepared by means of the sol-gel process, J. Mater. Sci. Mater. Med. 15 (2004) 457–461.

[8] X. Liu, P.K. Chu, C. Ding, Surface modification of titanium, titanium alloys and related materials for biomedical application, Mater. Sci. Eng. R 47 (2004) 49–121.

[9] I. Jirka, M. Vandrovcová, O. Frank, Z. Tolde, J. Plšek, T. Luxbacher, L. Bačáková, V. Starý, On the role of Nb-related sites of an oxidized β-TiNb alloy surface in its interaction with osteoblast-like MG-63 cells, Mater. Sci. Eng. C 33 (2013) 1636–1645.

[10] E. Fukada, I. Yasuda, On the piezoelectric effect of bone, J. Phys. Soc. Jpn. 12 (10) (1957) 1158–1162.

[11] E. Fukada, I. Yasuda, Piezoelectric effects in collagen, Jpn. J. Appl. Phys. 3 (2) (1964) 117–121.

[12] G.W. Hastings, F.A. Mahmud, The electromechanical properties of fluid filled bone: a new dimension, J. Mater. Sci. Mater. Med. 2 (2) (1991) 118–124.

[13] J.H. McElhaney, The charge distribution on the human femur due to load, J. Bone Joint Surg. 49A (1967) 1561–1571.

[14] S. Ramtani, Electro-mechanics of bone remodelling, Int. J. Eng. Sci. 46 (2008) 1173–1182.

[15] J.R. Fernández, J.M. García-Aznar, R. Martínez, Piezoelectricity could predict sites of formation/resorption in bone remodelling and modelling, J. Theor. Biol. 292 (2012) 86–92.

[16] F.R. Baxter, C.R. Bowen, I.G. Turner, A.C.E. Dent, Electrically active bioceramics: a review of interfacial responses, Ann. Biomed. Eng. 38 (6) (2010) 2079–2092.

[17] P. Vaněk, Z. Kolská, T. Luxbacher, J.A.L. García, M. Lehocký, M. Vandrovcová, L. Bačáková, J. Petzelt, Electrical activity of ferroelectric biomaterials and its effects on the

adhesion, growth and differentiation of human osteoblast-like cells, J. Phys. D. Appl. Phys. 49 (17) (2016) 175403.

[18] S. Itoh, S. Nakamura, M. Nakamura, K. Shinomiya, K. Yamashita, Enhanced bone ingrowth into hydroxyapatite with interconnected pores by electrical polarisation, Biomaterials 27 (32) (2006) 5572–5579.

[19] X.R.D.Software,https://www.bruker.com/products/x-ray-diffraction-and-elemental-analysis/x-ray-diffraction/xrd-software/topas.html2016.

[20] R.W. Cheary, A.A. Coelho, J.P. Cline, Fundamental parameters line profile fitting in laboratory diffractometers, J. Res. Natl. Inst. Stand. Technol. 109 (2004) 1–25.

[21] U. Welzel, J. Ligot, P. Lamparter, A.C. Vermeulen, E.J. Mittemeijer, Stress analysis of polycrystalline thin films and surface regions by X-ray diffraction, J. Appl. Crystallogr. 38 (2005) 1–29.

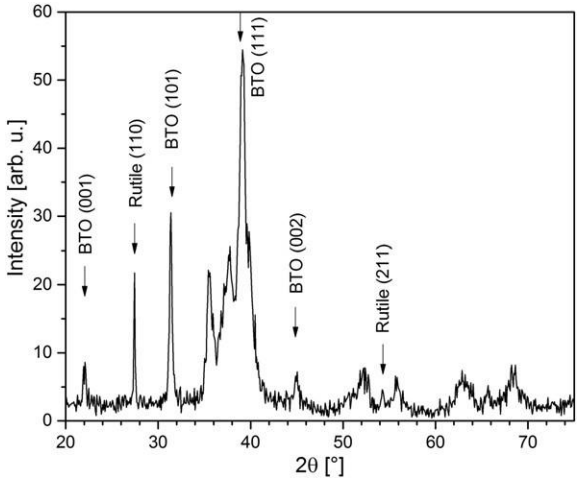

Fig. 1. XRD spectra of $BaTiO_3$/TiNb (1 Pa O_2, 2 J cm^{-2}, d_{T-S} = 35 mm, T_S = 700 °C, 120 nm).

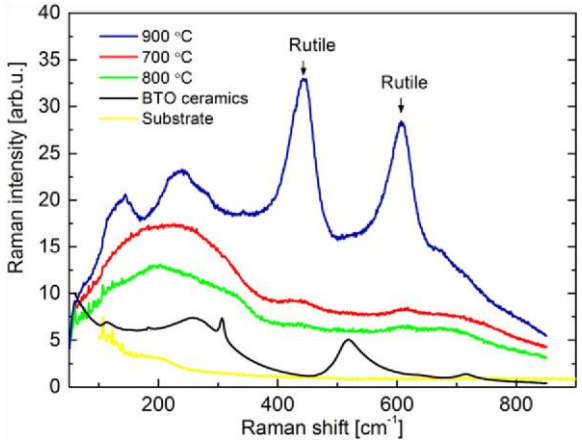

Fig. 2. Raman spectra of $BaTiO_3$/TiNb (T_S = 700 °C, 800 °C and 900 °C).

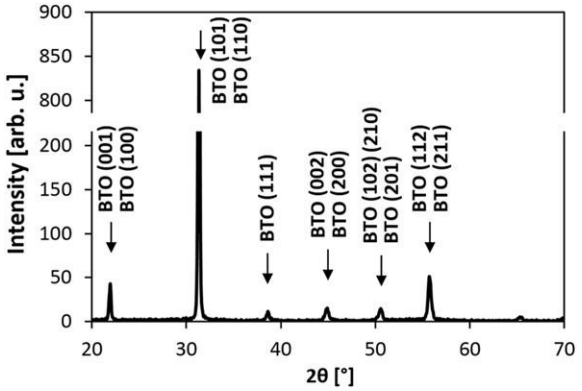

Fig. 3. XRD spectra of BTO/Si (100) (0.1 Pa O_2, d_{T-S} = 6 cm, T_S = 700 °C, 900 nm thick).

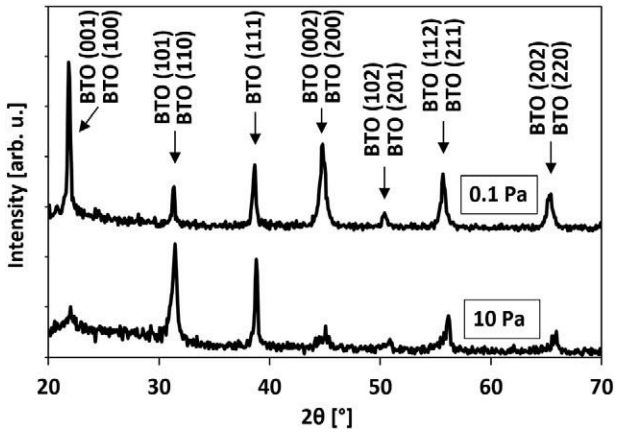

Fig. 4. XRD spectra of BTO/fused silica (T_S = 700 °C; 10 Pa O_2, 1080 nm and 0.1 Pa O_2, 910 nm).

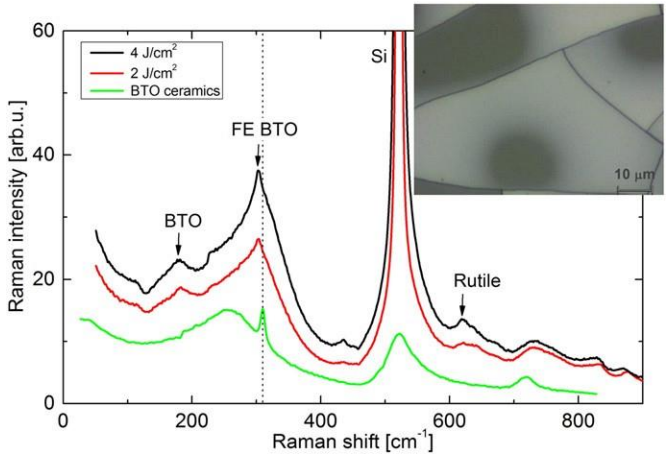

Fig. 5. Raman spectra of BTO/Si (100) (T_S = 700 °C; 2 J cm^{-2} and 4 J cm^{-2}) and BTO ceramics. FE BTO - the ferroelectric peak position.

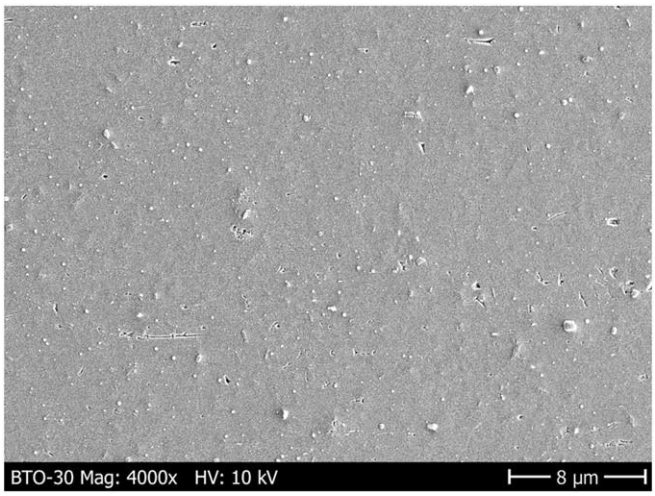

Fig. 6. SEM image of BTO/fused silica, (10 Pa O_2, T_S = 700 °C, $d_{T\text{-}S}$ = 6 cm, 1080 nm).

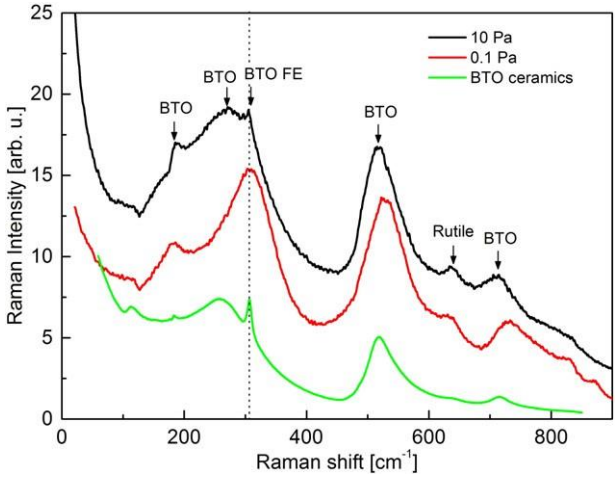

Fig. 7. Raman spectra of BTO/fused silica (T_S = 700 °C; 10 Pa and 0.1 Pa).

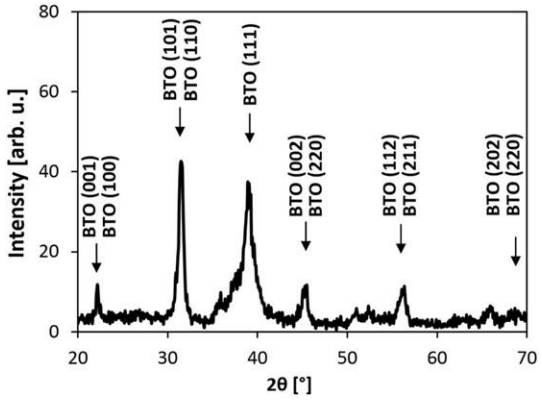

Fig. 8. XRD spectra of post-annealed BTO/TiNb (T_S = 160 °C, RTA for 4 min at 700 °C).

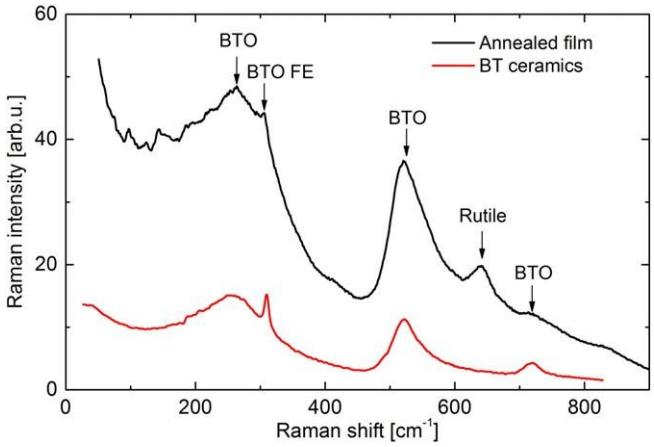

Fig. 9. Raman spectra of post-annealed BTO/TiNb (T_S = 160 °C, RTA for 4 min at 700 °C).

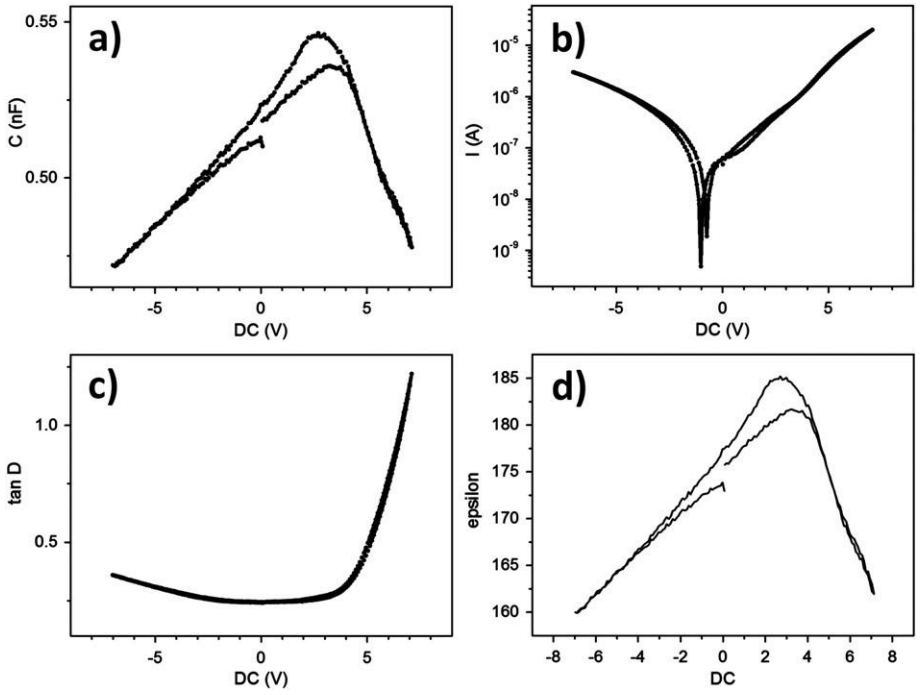

Fig. 10. Dielectric properties of the Pt/BTO/Pt/TiNb structure. (a) Capacitance, (b) leakage current, (c) loss factor and (d) epsilon as a function of dc voltage.

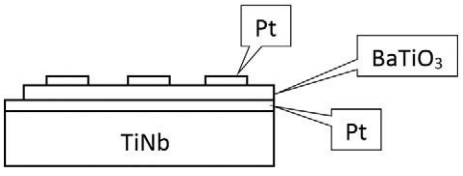

Fig. 11. Schematic cross-section of the BTO film sandwiched between Pt electrodes.

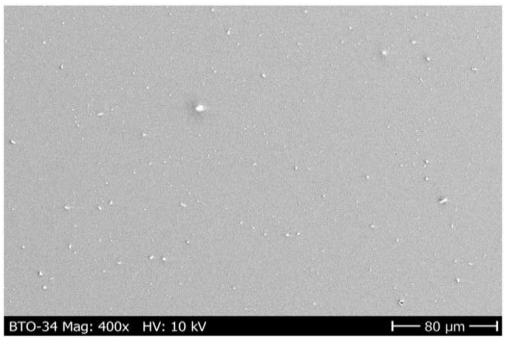

Fig. 12. SEM image of Pt/BTO/Pt/TiNb structure (10 Pa O_2, d_{T-S} = 6 cm).

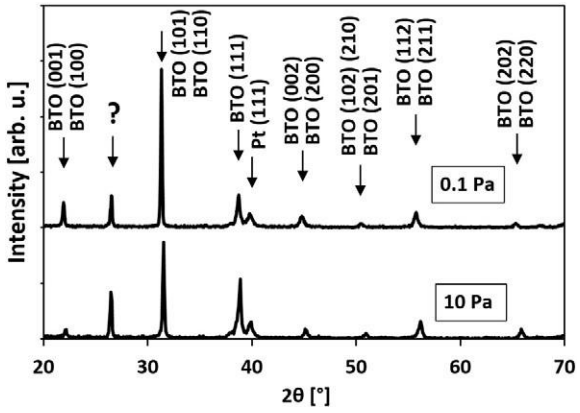

Fig. 13. XRD spectra of Pt/BTO/Pt/TiNb structure (d_{T-S} = 6 cm; 10 Pa O_2 and 0.1 Pa).

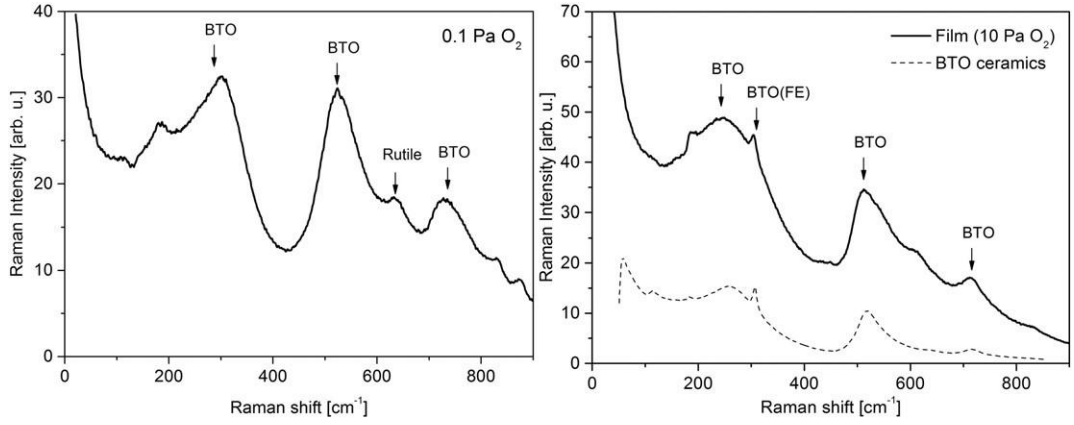

Fig. 14. Raman spectra of BTO/TiNb (T_S = 700 °C, 0.1 Pa and 10 Pa).

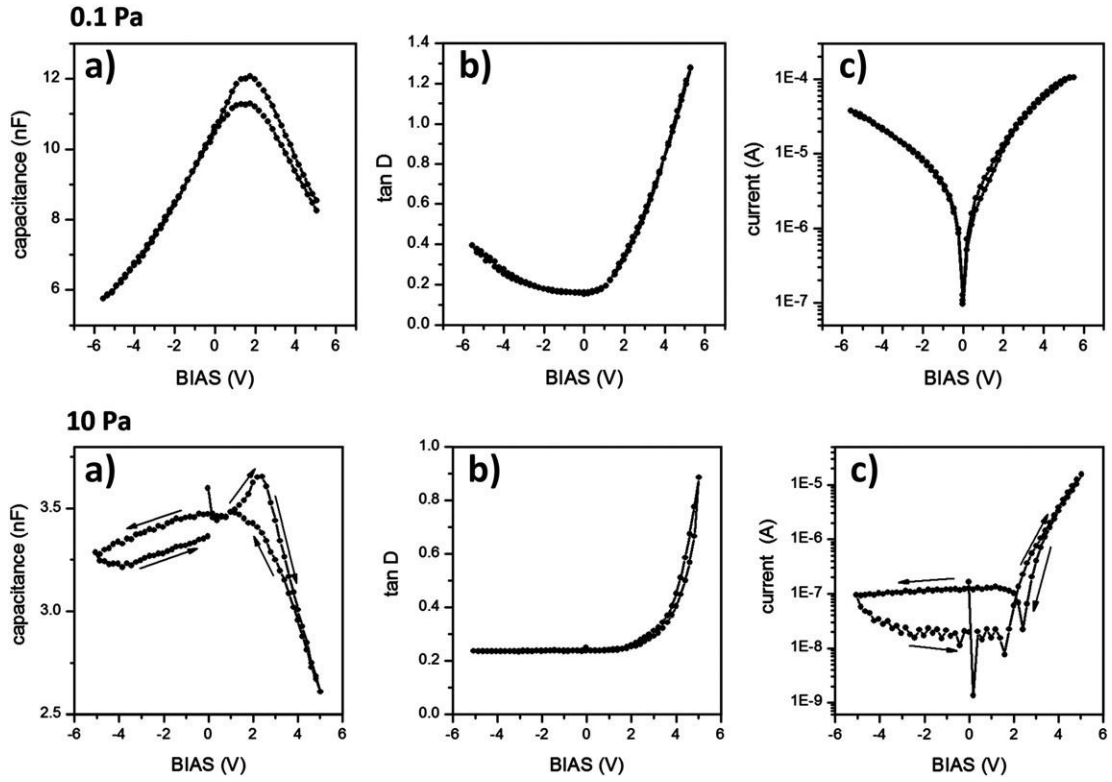

Fig. 15. Dielectric properties of Pt/BTO/Pt/TiNb structure (0.1 Pa O_2 and 10 Pa). (a) Capacitance, (b) loss factor, (c) leakage current against dc voltage.